PHYSICAL REVIEW B VOLUME 17, NUMBER 8 15 APRIL 1978

New magneto-optical anomalies of impurity electrons in InSb at the two-LO-phonon region: Theory and experiment*

J. T. Devreese
University of Antwerpen (RUCA and UIA), c/o Groenenborgerlaan 171, 2020 Antwerpen, Belgium

J. De Sitter
University of Antwerpen (RUCA), Groenenborgerlaan 171, 2020 Antwerpen, Belgium

E. J. Johnson
GTE Laboratories, Waltham, Massachusetts 02154

K. L. Ngai
Naval Research Laboratory, Washington, D.C. 20375

(Received 3 August 1977)

We present both experimental magneto-optical measurements and a theoretical analysis of polaron anomalies observed when impurity electron excitations are resonant in energy with two long-wavelength LO phonons. Specifically, we have measured the first harmonic of impurity cyclotron resonance (HCR) and the LO-phonon assisted cyclotron resonance transition (LOCR) in InSb in the magnetic field range 27–60 kG. In this range the HCR is nearly twice the LO-phonon energy, and the LOCR is close to the HCR. When the magnetic field is swept through this range, we have observed dramatic polaron pinning effects that are quite different from those ordinarily observed in the one LO-phonon region. For example, the line intensity of the LOCR anomalously disappears in the resonant interaction region but regains its intensity at either lower or higher fields. This feature is just opposite to the polaron pinning effects in the one LO-phonon region. In addition, we have calculated the magneto-optical spectrum of donor-impurity electrons taking into account nonparabolicity, impurity-electron energy-level scheme, and polaron interactions between the HCR, LOCR, and the lowest set of impurity states with participation of up to two LO phonons. We demonstrate that by using the nonparabolic-energy-level scheme, the wave functions of donor electrons, and the known Fröhlich interaction constant between electrons and LO phonons, we can explain the anomalous features of the present data quantitatively without any adjustable parameters.

I. INTRODUCTION

Electronic energy levels in polar crystals are shifted by the electron-phonon interaction. These perturbations are called polaron effects.[1,2] Such effects will be magnified and particularly easy to observe when a pair of levels has energy separation close to the long-wavelength LO-phonon energy $\hbar\omega_0$.[3]

In some polar crystals it is possible to tune the separation of a pair of electronic levels by means of an applied magnetic field or stress. One then observes the magnitude of the relative energy shift and the line-shape changes as the hypothetical separation of the unshifted levels approaches $\hbar\omega_0$ from above or below. Experiments of this kind demonstrate a characteristic discontinuity of the level separation at $\hbar\omega_0$ accompanied by a broadened and sometimes asymmetrical upper branch. This phenomenon has been called the polaron-pinning effect.[3-7]

Polaron-pinning effects were first observed by Johnson and Larsen in the interband magnetoabsorption in InSb.[3] Later, shallow donor levels in InSb were found to display similar kinds of discontinuities.[4] The study of polaron effects has been extended to other materials like CdTe,[8] $Hg_xCd_{1-x}Te$,[7] and p-type InSb.[9] The development of the field and its present status have been reviewed recently by different authors.[6,7,10,11]

In the past, all the work on polaron-pinning effects that involve LO phonons has been restricted to the participation of only a single LO phonon, where the region of interest is indicated as the shaded area labeled A in Fig. 1. However, intense lattice absorption near the reststrahl frequency has limited cyclotron-resonance studies, for example, to the fringes of the region of interest. Studies which utilize interband magnetoabsorption[3] and combined cyclotron resonance[6,7,12] have overcome this difficulty. In earlier experiments[13] we have demonstrated that infrared absorption with photon energies below 30 meV (region D of Fig. 1) involving LO-phonon assisted cyclotron resonance[14-16] and harmonics of cyclotron resonance[17-19] occurs in significant strength in InSb. We have also studied both of these transitions in the nonpolar two-optical-phonon energy region.[20] In the present experiments, we have examined such absorption in detail in the two-LO-

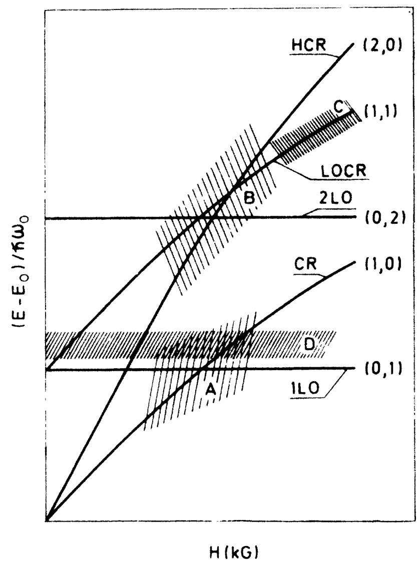

FIG. 1. Schematic plot of the hypothetical magneto-optical spectra in the absence of polaron interaction. The shaded region A has been, in the past, extensively studied and corresponds to the conventional polaron-pinning effects of Johnson and Larsen (Ref. 3). Our present interest is in the shaded region B.

phonon energy region, indicated as the region B in Fig. 1. In this energy range the lattice absorption does not overwhelm the electronic absorption. Moreover, as we shall further demonstrate in Sec. II, only the LOCR transition has significant absorption intensity in region C. In the present work, we present both experimental measurements and theoretical analysis on polaron effects when two long-wavelength LO phonons participate simultaneously in pinning. Specifically we measured in region B of Fig. 1 the first harmonic of the cyclotron resonance transition and the LO-phonon assisted cyclotron resonance transition in InSb in the magnetic-field range of 27–60 kG. In this magnetic-field range the first harmonic of cyclotron resonance (HCR) is separated in energy from the ground-state level by nearly $2\hbar\omega_0$, the two-LO-phonon energy, while the LO-phonon assisted cyclotron resonance (LOCR) is also close in energy to the HCR. When the magnetic field is swept across this range, we can expect novel polaron-pinning effects to be observed. Further, at this relatively high energy, nonparabolicity of the electronic energy levels is significant and will play an important role. We shall also see that the electronic-impurity-level scheme reflects itself on the detail of the magneto-optical spectrum. In Sec. II the experimental procedure and data will be presented. Theoretical calculations of the magneto-optical spectrum, taking into account nonparabolicity, the impurity-electronic-level scheme, and polaron interactions between the HCR, LOCR, and the lowest set of impurity levels with participation up to two LO phonons will be presented in Sec. III. We shall demonstrate that, by using the energy-level scheme and wave functions of donor electrons previously determined by comparison between theory and experiment and the known Fröhlich interaction constant[1] between electrons and LO phonons, all the anomalous features of the present data can be explained without any other adjustable parameters.

II. EXPERIMENT

A. Experimental procedure

The experiments consisted essentially in examining the infrared transmission of an InSb sample at appropriate magnetic fields and temperature. Certain procedures were used to distinguish between the magnetically induced absorption and the background two-phonon lattice absorption.

The sample was tellurium doped with $n = 1.4 \times 10^{15}$ cm^{-3} and $\mu(77\,°\mathrm{K}) = 3 \times 10^5$ cm/sec. The thickness was 1.87 mm. For most of the measurements the sample was oriented with the magnetic field in the [110] direction and the propagation vector of the light was perpendicular to the magnetic field. The sample temperature was controlled using helium exchange gas and liquid helium. The temperature was 6 °K which is in the region where carriers freeze out onto impurities and impurity-electron transitions have to be considered. Magnetic fields from 10 to 80 kG were provided by a superconducting solenoid. The magnetic field range and the energy range are covered up to about 65 kG and 70 meV, respectively. The infrared transmission in this range of an InSb sample at 6 °K and zero magnetic field was measured (Fig. 2). We were concerned with

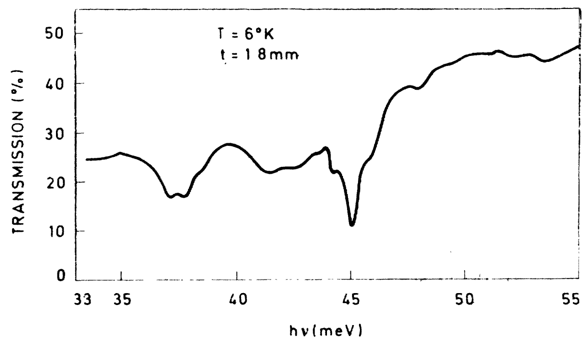

FIG. 2. Infrared transmission of n-InSb at 6 °K and zero magnetic field.

the problem of isolating the absorption that appears in this region with the application of appropriate magnetic fields. The absorption that is induced by the application of a magnetic field corresponds to about a 10–15% modulation of the transmission at zero magnetic field.

We have used two approaches to isolate the induced absorption. (i) Fix frequency and scan magnetic field. Under the assumption that the lattice absorption is independent of the magnetic field, any structure that is observed is attributed to the magneto-absorption of electrons. (ii) Fix magnetic field and scan energy. At the same time obtain data similar to Fig. 2 and plot the ratio. The structure in the resulting spectrum is attributed to the electronic magneto-absorption i.e.,

$$\frac{T(B)}{T(0)}=\frac{1-R^2e^{-2\alpha(0)x}}{1-R^2e^{-2\alpha(B)x}}\,e^{-[\alpha(B)-\alpha(0)]x} \tag{1a}$$

where $T(0)$ and $\alpha(0)$ are, respectively, the transmission and absorption coefficients in the absence of an external magnetic field, whereas $T(B)$ and $\alpha(B)$ are the corresponding quantities when an external magnetic field B is applied. R is the reflection coefficient and x is the sample thickness. The ratio before the exponential in Eq. (1a) is significantly different from unity only at high transmissions. At $T(0)=25\%$ and induced absorption equal to the lattice absorption, the ratio differs from unity by only 3%. However, making a ratio of data by hand calculation is tricky and quite formidable. In the approach we have used, the data are stored on magnetic tape and the ratio is calculated via computer. In using this approach one must be careful that the calibration corresponds correctly point for point between the two scans. In our case the calibration on each scan was checked every 0.043 meV.

These two approaches are not equivalent but supplement each other. Structure that can be observed with one approach is not always observed with the other. In the magnetic-field scan, difficulties can occur when both the intensity and the energy position of an absorption line vary with magnetic field. Difficulties occur when the position of a magneto-absorption peak becomes independent of magnetic field in some magnetic-field range.

B. Experimental results

We first show a plot of the energy positions (as open circles) of the entirety of the observed peaks that can be resolved versus magnetic field in Fig. 3. The lines in this figure are drawn arbitrarily through the data points to guide the eyes and for easy reference and may have no physical significance. Apparent gaps as indicated in Fig. 3 where there are no data points are real and are due to lack of appreciable absorption intensity such that the peak cannot be resolved, not to lack of measurements there. We could expect data points on the lower line to be second harmonic cyclotron resonance. However, data at lower energies analyzed in a previous paper[13] (not shown) show clearly that the second haromonic cyclotron resonance dies out before these energies are reached and the data points on the lower line are to be associated with the phonon-assisted cyclotron resonance (LOCR), with the energy equal to the sum of cyclotron energy $\hbar\omega_c$ and an LO phonon energy

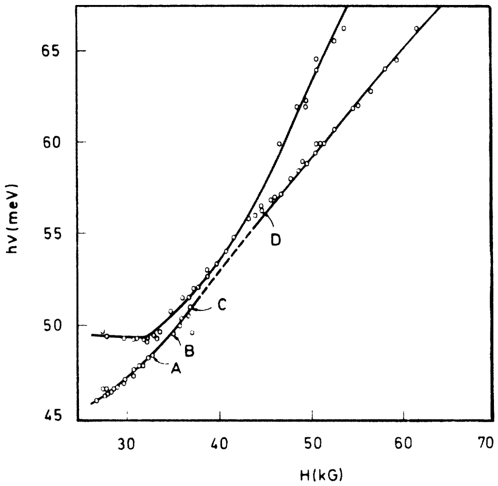

FIG. 3. Plot of the energies of the resolved absorption peaks (open circles) versus magnetic field. Apparent gaps of open circles between A and B and also between C and D are due to weak absorption intensity at these gaps and not to lack of measurements there. The lines in the figure are arbitrarily drawn to guide the eyes.

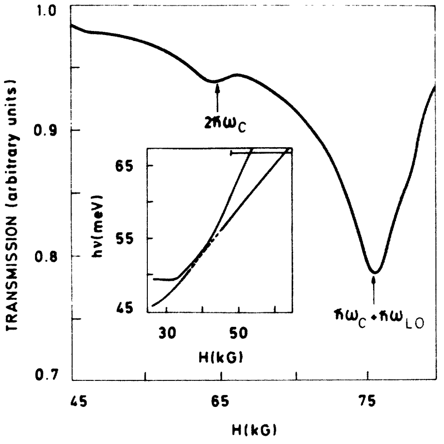

FIG. 4. Magnetic-field scan spectrum at 67.5 meV.

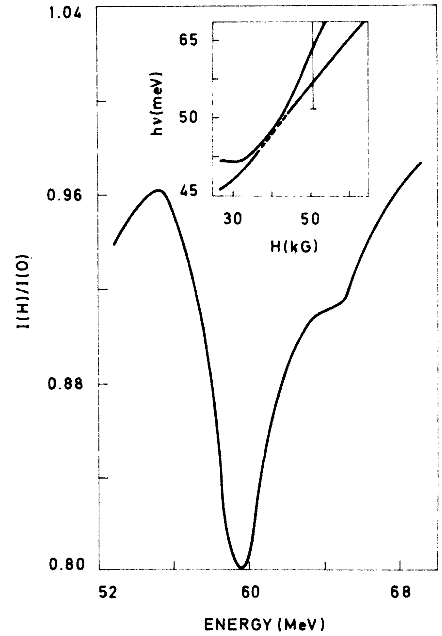

FIG. 5. Energy scan spectrum at 51 kG.

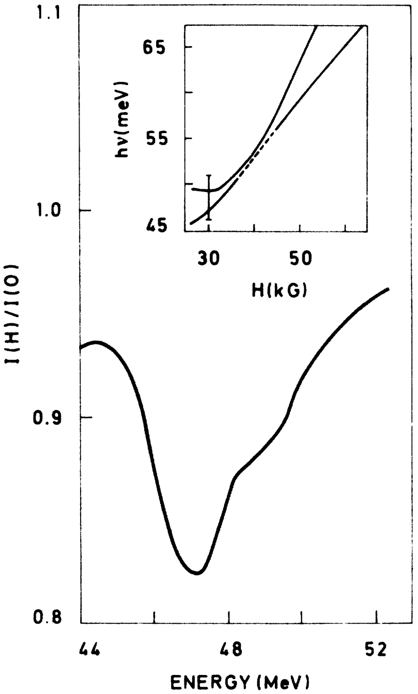

FIG. 6. Energy scan spectrum at 30 kG.

$\hbar\omega_0$. The high energy end of the upper line can be the second harmonic cyclotron resonance (HCR), $\approx 2\hbar\omega_c$, while the low-energy flat portion is nearly $2\hbar\omega_0$ and represents two-LO-phonon excitations (2LO). Other than these possible indications, the data are too complex especially in the interaction region and obviously no ready interpretation can be made. The data in a sense are even more perplexing in the anomalous variations of the line shapes and intensities of the absorption peaks represented by the data points. These aspects will be discussed in the following paragraphs.

In Fig. 4 we show a magnetic-field scan with a fixed photon energy of 67.5 meV, i.e., at considerably higher energy than that where the anomalies occur. Here the dominant absorption is the lower line of Fig. 3 which can be identified as the LOCR transition. In the figure the peaks are labeled $2\hbar\omega_c$ and $\hbar\omega_c+\hbar\omega_{\text{LO}}$. These labels should be taken as equivalent to the HCR and the LOCR notations. In Fig. 5, we show an energy scan at a fixed magnetic field of 51 kG, again in the high-energy region. In this case the HCR shows up as a weak shoulder and the LOCR transition dominates.

Consider next the low-energy (magnetic field 27–30 kG) region sufficiently removed from the anomalies. Frequency scans at fixed field show that the lower line of Fig. 3, which can be again identified as the LOCR transition, dominates in intensity. An example is shown in Fig. 6 where the energy scan is at a fixed magnetic field of about 30 kG. These observations in both the high- and low-energy region, where anomalies due to polaron interaction are expected to have a minor effect, lead us to establish that in the entire energy and field ranges of 45–67.5 meV and 27–65 kG, respectively, had there been no polaron interactions, the unperturbed LOCR transition would

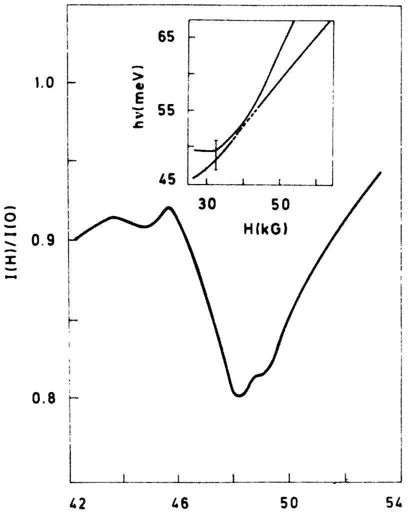

FIG. 7. Energy scan spectrum at 32.5 kG.

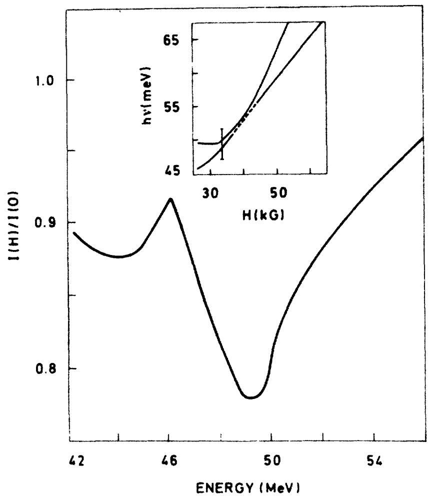

FIG. 8. Energy scan spectrum at 33.5 kG.

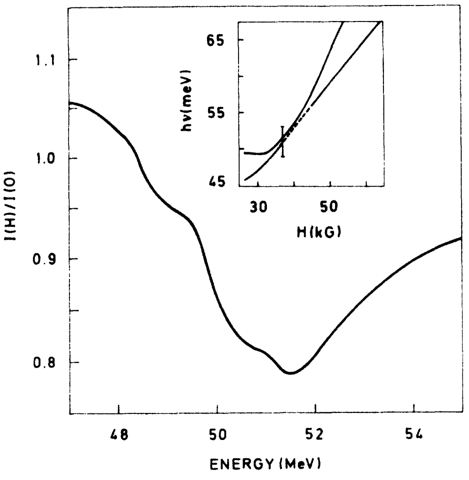

FIG. 10. Energy scan spectrum at 37 kG.

have dominated in absorption intensity. In the perturbation region where the anomalies have important modifications of the magneto-optical spectra, the LOCR is perturbed and its absorption intensity appears to be transferred to other transitions.

We now present the data in the interaction region (30–50-kG region). Figure 7 is an energy scan at $H = 32.5$ kG where two peaks at near 48 meV of approximately equal intensity are resolved. At slightly higher fields, the two peaks cannot be resolved anymore. Figure 8 taken at $H = 33.5$ kG illustrates this situation which is referred to as the gap between A and B of the lower line in Fig. 3. The broad peak occurs at energy close to the upper line (Fig. 3). At fields $H \geq 36$ kG, two peaks of approximately equal strength can again be resolved as shown in Fig. 9. At $H = 37$ kG, three peaks can be resolved (Fig. 10). At slightly higher field, the energy scan reveals only one broad peak at a fixed magnetic field and is referred to as the gap of data points between C and D of the lower line in Fig. 3. Examples of this behavior are illustrated by Figs. 11–13. In these plots the peak position appears to shift continuously from the upper line to the lower line of Fig. 3. Returning for the moment to Fig. 5 at 51 kG, we see that as H is further increased the lower line of Fig. 3 regains its intensity and dominates the upper

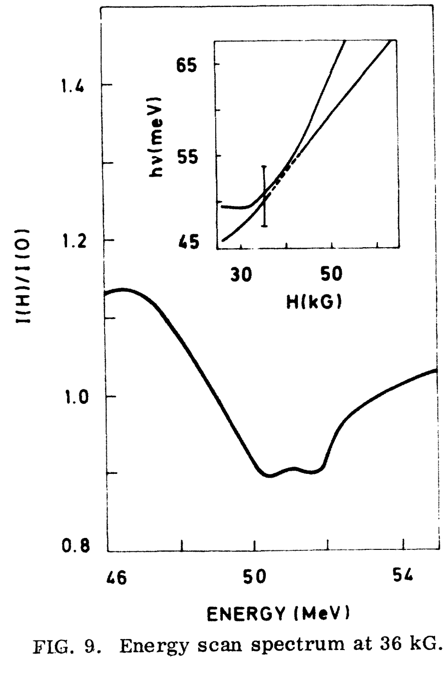

FIG. 9. Energy scan spectrum at 36 kG.

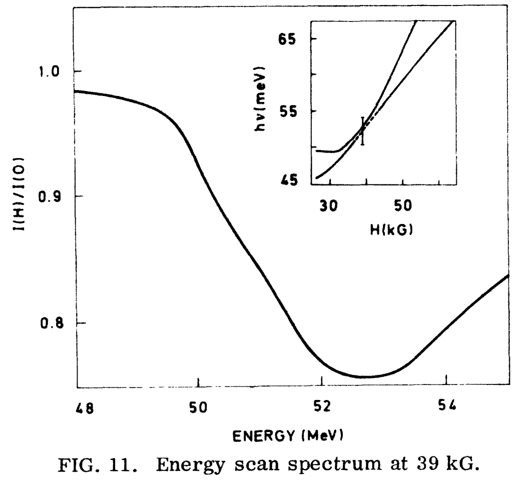

FIG. 11. Energy scan spectrum at 39 kG.

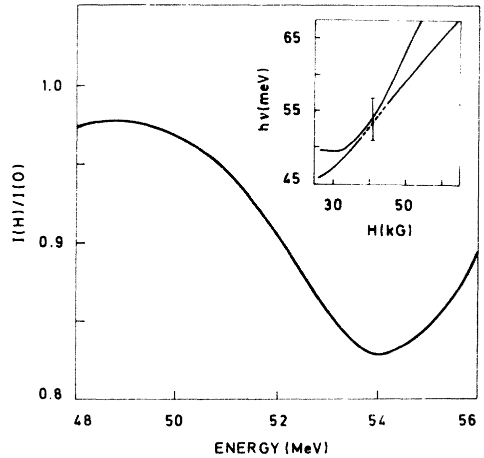

FIG. 12. Energy scan spectrum at 41 kG.

line which is observed as a weak shoulder. The anomalies of the magneto-optical spectra as described are too complex in spite of the fact that we have taken and displayed a lot of data. The anomalies include the disappearance of the lower line (Fig. 3) at midfield range and its reappearance at higher fields and are quite different from conventional polaron-pinning observations in the one-LO-phonon region. It is by now clear that it is not useful to further discuss the data without theoretical considerations. Hence we shall present the rest of the data in Sec. III after the theoretical analysis has been performed.

III. THEORY

It would be helpful as a first step for understanding the details and the data to calculate the noninteracting energy levels for the first HCR and the LOCR and their positions relative to the two LO phonons (2LO). To accomplish this, we employ the results of two earlier calculations. One of these is the calculation by Johnson and Dickey[13] of the conduction-band energy levels as deduced from experiments involving cyclotron resonance, combined resonance, and the spin resonance and forcing the experimental results to agree within 1% with the calculations of the energy levels using a band-edge effective mass of 0.0139 and a band-edge g factor of −51.3. This approach yields a cubic equation which includes the nonparabolic effects resulting from the interaction of the conduction band with the three valence bands. Once these magnetic band energy ($k_z = 0$) levels $|N=1,4\rangle$, $|N=2,4\rangle$, and $|N=0,4\rangle$ are obtained as a function of magnetic field, we use the results of another calculation of the donor impurity states binding energies by Lin-Chung and Henvis,[21] which employs the nonparabolic scheme of Groves and Pidgeon[22] and the variation calculation method of Wallis and Bowlden,[23] to obtain finally the donor-impurity-electron-state energies. Although Ref. 21 gives also the absolute energies of the donor states, we employ Johnson and Dickey's magnetic-band-edge calculations because they are in better agreement with experiment. The level scheme (not to scale) of the donor levels is illustrated in Fig. 14. The bound-donor states ($NM\gamma$) have the variational envelope wave function

$$F(N,M,\gamma)=f(N,M)P_\lambda(z)e^{-(1/4)\gamma\epsilon^2 z^2}, \qquad (1b)$$

where $f(N,M)$ are free-charge-carrier envelope functions, ϵ is the variational parameter, and γ is the magnetic field parameter defined by $\gamma=\frac{1}{2}\hbar\omega_c/R^*$, the ratio of half the cyclotron frequency to the effective Rydberg. $P_\lambda(z)$ represents a set of ortho-

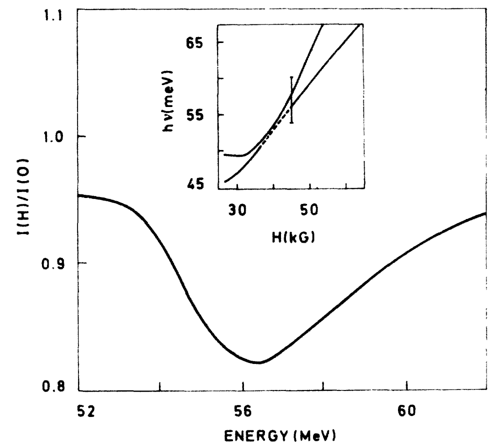

FIG. 13. Energy scan spectrum at 45 kG.

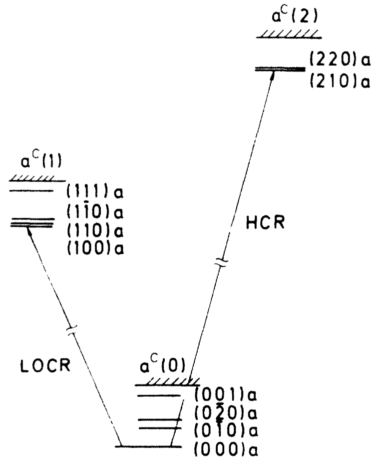

FIG. 14. Impurity levels and associated impurity HCR and LOCR transitions (schematic).

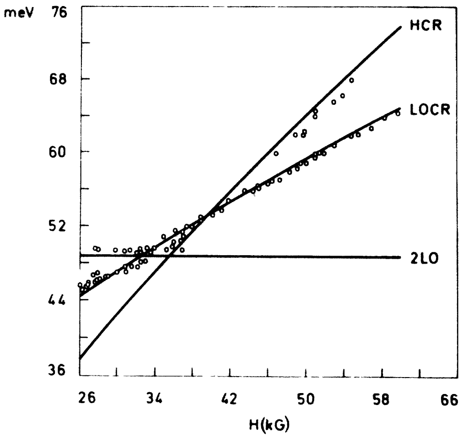

FIG. 15. Data points as in Fig. 3 together with the noninteracting HCR and LOCR impurity transitions as defined in Fig. 14 shown as solid lines.

gonal polynomials of argument z of order λ. It was assumed that the magnetic field is chosen to be along the z direction.

The HCR and LOCR transitions observed and reported in this work are also indicated schematically in Fig. 14. We have computed these noninteracting transition energies as a function of field in the region of interest and the results are displayed in Fig. 15 as the solid lines together with the data points. We can now compare these noninteracting HCR and LOCR transitions with the data and readily deduce the following initial conclusions. From the near coincidence of the calculated values of the HCR at high fields and LOCR at both low and high fields with some of the data points, we can establish: (i) that the experimental observed transitions are indeed the HCR and LOCR transitions; (ii) that the LOCR transition dominates in intensity at both the low and the high ends of the magnetic-field region B of Fig. 1; (iii) that the HCR at the low end of the field region is not observed and this is consistent with the weak HCR transition intensity in region B of Fig. 1 and also at higher fields.

We can also pick out some of the outstanding anomalies. (a) The intensity of the LOCR decreases as the magnetic field increases from 28 kG, almost completely loses its intensity around 40 meV with the emergence of another yet unidentified peak, and finally at about 45 meV regains its prominence. (b) Another branch of data points appears at or below 32 kG that seems to be pinned at twice the LO phonon energy and to have an intensity which rapidly attenuates as we move to lower fields.

To explain these novel features of the magneto-optical spectrum, we proceed to calculate the interacting HCR, LOCR, and also the level 2LO corresponding to the ground state with the presence of two LO phonons. We shall specify these states in detail after the presentation of the scheme for calculating of LO-phonon interactions between the levels. The levels interact via the Fröhlich Hamiltonian H, in the presence of an external magnetic field. The total Hamiltonian is

$$H=H_0+H_1\,, \tag{2}$$

$$H_0=\left(\vec{p}+\frac{e}{c}\vec{A}(\vec{r})\right)^2+\sum_{\vec{q}}\hbar\omega_{\vec{q}}\,b^\dagger_{\vec{q}}b_{\vec{q}}\,, \tag{3}$$

$$H_1=\sum_{\vec{q}}\hbar\omega_{\vec{q}}\left(\frac{4\pi\alpha}{S}\right)^{1/2}\frac{1}{r_0 q}\,(e^{-i\vec{q}\cdot\vec{r}}b^\dagger_{\vec{q}}+\text{H.c.})\,, \tag{4}$$

where

$$S=V/r_0^3\,,\quad r_0=(\hbar/2m^*\omega_q)^{1/2}\,,$$

m^* is the band mass, and α the polaron coupling constant which has the value of 0.02 for InSb. $b^\dagger_k$ creates an LO phonon of wave vector $\vec{k}$ and it is assumed that there is no dispersion i.e., $\omega_q=\omega_0=$ constant.

The unperturbed states of Eq. (2) are taken to be eigenstates of H_0. As we have discussed, the donor electronic states are described by the set of quantum numbers $(Nm\lambda)$ which will be abbreviated by the notation ξ. We focus attention on zero-phonon eigenstates $|\xi;0\rangle$, one-phonon eigenstates $|\xi;q\rangle$, and two-phonon eigenstates $|\xi;q,q'\rangle$ where

$$H_0\,|\xi_0,0\rangle=E_{\xi_0}\,|\xi_0,0\rangle\,, \tag{5}$$

$$H_0\,|\xi_1;q\rangle=(E_{\xi_1}+\hbar\omega_0)\,|\xi_1;q\rangle\,, \tag{6}$$

and

$$H_0\,|\xi_2;q,q'\rangle=(E_{\xi_2}+2\hbar\omega_0)\,|\xi_2;q,q'\rangle\,. \tag{7}$$

For applications to our problem, the electronic states that occur in the two-phonon eigenstate $|\xi_2;q,q'\rangle$ can be (000), (0$\bar{1}$0), and (0$\bar{2}$0), etc. (Fig. 14). While the states ξ_1 in the one-phonon state (LOCR) can be (100), (110), and (1$\bar{1}$0), etc. Similarly the states ξ_0 in the zero-phonon state (HCR) are (210) and (220), etc. Clearly H_1 couples together zero-phonon, one-phonon, and two-phonon states. In the magnetic-field range of present interest, it happens that their energies

$$E_{\xi_0}\approx E_{\xi_1}\approx E_{\xi_2} \tag{8}$$

are very close to each other; then even if α is small the corresponding exact eigenstates of H can be quite different from $|\xi_0;0\rangle$, $|\xi_1;q\rangle$, and $|\xi_2;q,q'\rangle$. The perturbed wave functions will be given.

An LOCR level $|\xi_1;q\rangle$ as an unperturbed state consists of an electron at state ξ_1, together with an LO phonon. It is coupled via the Fröhlich

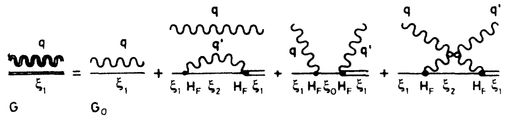

FIG. 16. Diagrammatic representation of the interacting LOCR Green's function.

interaction H_1 to other states. The Green's function for the LOCR state is given by

$$G_{\xi_1,\vec{q}}(E) = 1/[E - E_{\xi_1} - \hbar\omega_0 - \Sigma(E)] \tag{9}$$

where $\Sigma(E)$ is the self-energy.

The LOCR interacting Green's function $G_{\xi,\vec{q}}$ is given in terms of the noninteracting $G^{(0)}_{\xi_1,\vec{q}}$ by Eq. (9) rewritten as

$$G^{-1}_{\xi_1,\vec{q}} = (G^{(0)}_{\xi_1,\vec{q}})^{-1} - \Sigma \ . \tag{10}$$

This is diagrammatically expanded in Fig. 16 where the self-energy arises from the Fröhlich interaction H_1 as depicted by the heavy dots.

For InSb the interaction H_1 is weak and we can immediately obtain the perturbative result

$$G^{-1}_{\xi_1,\vec{q}}(E) = E - E_{\xi_1} - \hbar\omega_0 - \sum_{\xi_2 q'} \frac{|\langle \xi_1;\vec{q}\,|H_1|\,\xi_2;\vec{q},\vec{q}\,'\rangle|^2}{E - E_{\xi_2} - 2\hbar\omega_0}$$

$$- \sum_{\xi_0} \frac{|\langle \xi_1;\vec{q}\,|H_1|\,\xi_0;0\rangle|^2}{E - E_{\xi_0}} \ . \tag{11}$$

The expression in Eq. (11) for $G^{-1}_{\xi_1,\vec{q}}(E)$ is obtained from Fig. 16 by replacing the full Green's function by $G^{(0)}_{\xi_1,\vec{q}}$, and at the same time retaining the contributions from $q' = q$ terms only in the last two diagrams. These approximations are equivalent to those made in the method given in Appendix A and the results of Eq. (11) are identical to those of Eqs. (A3)–(A6). It turns out that Eq. (10) can be solved exactly without making these approximations. The exact solutions introduce extra structures into the magneto-optical spectrum in addition to that given by the present approximate results of Eq. (11). These extra structures will not be able to be resolved by the experimental procedures adopted here. Hence we shall consider the perturbation result of Eq. (11) for the remainder of this work.

The energy locations E_1 of the interacting levels $|\,\xi_0;0\rangle$, $|\,\xi_1;\vec{q}\rangle$, and $|\,\xi_2;q,q'\rangle$ can be obtained as the set of poles $\{E_i\}$ of $G_{\xi_i,\vec{q}}$ (or zeros of $G^{-1}_{\xi,\vec{q}}$). The spectral function $A(E)$

$$A(E) = \sum_i A(E - E_i) = (-1/\pi)\,\mathrm{Im}\,G_{\xi_1,\vec{q}}(E_i)$$

$$= \left(\frac{\partial G^{-1}_{\xi_1,\vec{q}}}{\partial E}\right)^{-1}\Bigg|_{E=E_i} \delta(E - E_i) \tag{12}$$

gives the weight W_i of the $|\,\xi_1;q\rangle$ state character in the branch E_i as

$$W_i = [\partial G^{-1}_{\xi_i;\vec{q}}(E)/\partial E]^{-1}\big|_{E=E_i} \ . \tag{13}$$

It can be verified by straightforward though tedious algebra that

$$\sum_i W_i = 1 \tag{14}$$

and W_i is related to the coefficients $b(\xi_i;\vec{q})$ in Eq. (A6) of Appendix A by

$$W_i = K\,|\,b(\xi_1;\vec{q})|^2\,\big|_{E=E_i} \tag{15}$$

with K being a renormalization constant.

Calculations of the weights W_i are necessary for comparison with the intensities of the various E_i branches. W_i are direct measures of the distribution of the LOCR transition intensity into the various interacting levels E_i. This procedure is based on the fact that, in the experimental region of 28–60 kG, the LOCR transition dominates in intensity to such an extent that the noninteracting HCR transition is not even observable or weakly observable except near the resonance region $E_{\xi_0} \approx E_{\xi_1} + \hbar\omega_0$. Hence we can neglect the intensity contributions to the branches E_i from the HCR and W_i of Eq. (13) gives a good description of the various branches as a function of magnetic field.

IV. CALCULATIONS

Before we present the most detailed calculation for the magneto-optical spectrum and its intensities, we examine some simplified and at times even hypothetical calculations. We do so for at least two reasons. One reason for use of the hypothetical calculation is to elucidate some of the physical features that are retained even in the results of the detailed calculations. Another reason is to demonstrate the inadequacy of simplified or hypothetical calculations so as to bring out the importance of effects like nonparabolicity, and donor excited state levels $|\,\xi_0;0\rangle$.

A. Parabolic band

This is a hypothetical case in which we consider three levels which have the field dependences

$$E_{\xi_0} = 2\hbar\omega_c \ ,$$

$$E_{\xi_1} = \hbar\omega_c + \hbar\omega_0 \ ,$$

$$E_{\xi_2} = 2\hbar\omega_0 \ ,$$

where $\omega_c = (eH/m^\star c)$ is the cyclotron frequency with $m^\star$ taken as constant (hence like a parabolic band). The three levels are simultaneously degenerate at $\omega_c = \omega_0$. When the Fröhlich interaction is switched on, the resulting energy levels are given by the zeros of $G^{-1}_{\xi,\vec{q}}$ of Eq. (11) and are plot-

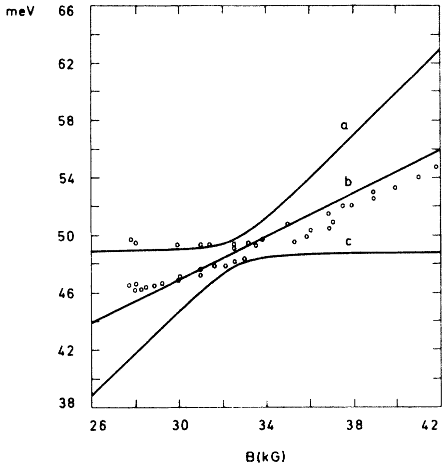

FIG. 17. Interacting levels scheme for the case of a parabolic band.

ted as solid lines in Fig. 17. Their LOCR spectral weights W_i are given in Fig. 18. It must be pointed out from the outset that the relatively good fit to the data points in Fig. 17 is of course meaningless because we have arbitrarily adjusted the effective mass to be 0.015 of a free-electron mass. However, the interesting features are that three branches appear and that polaron-pinning effects similar though distinct from the one-LO-phonon effect are present. For instance, the intensity of the b branch, which corresponds to the LOCR transition $|\xi_1;q\rangle$ when far away from the $\omega_c=\omega_0$ anomaly, decreases and vanishes at the field when $\omega_c=\omega_0$, while both branches a and c regain considerable intensity only near that field value.

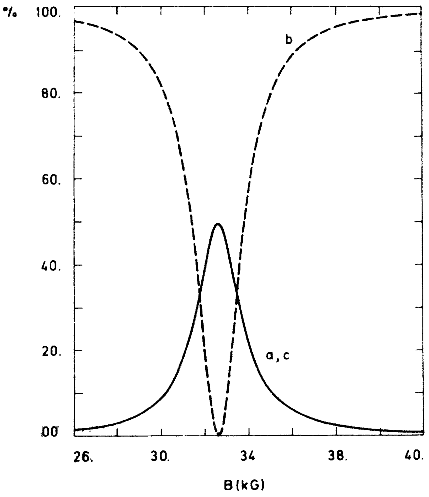

FIG. 18. Absorption intensities of the levels of Fig. 17.

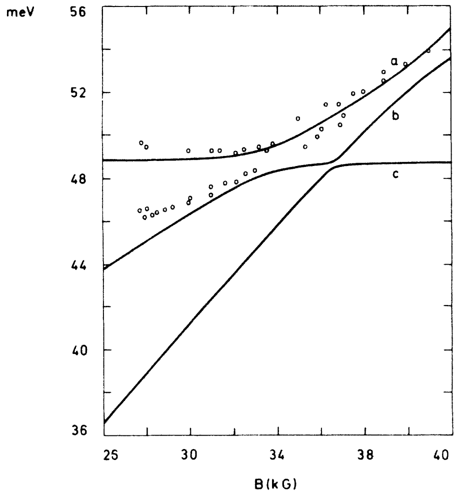

FIG. 19. Interacting levels scheme for Landau-level continuum levels with nonparabolicity taken into consideration.

This feature resembles the behavior of the data discussed earlier in Sec. II. On the other hand, although the calculated branches a, b, and c correlate reasonably well with the data points, yet the intensity variation is rather poor. As we shall see this is primarily due to nonparabolicity.

B. Nonparabolic band

In this case we take the three levels as in Sec. IV A, except that E_{ξ_0}, E_{ξ_1}, and E_{ξ_2} are the energies of the bottoms ($k_z=0$) of the $N=2$, $N=1$, and $N=0$ Landau continuum, respectively, calculated from the nonparabolic theories. The branch positions calculated (Fig. 19) correlate well with the data

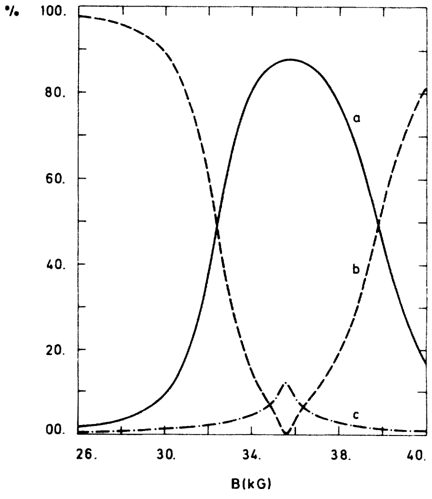

FIG. 20. Absorption intensities of the levels of Fig. 19.

points except at near 28 kG, where the b branch is significantly below the data. The spectral weights W_i (Fig. 20) retain the general features of Fig. 18. There is a serious difficulty, however, when the data points for $B > 38$ kG are interpreted as the a branch as suggested by Fig. 19, because this contradicts the result of Fig. 20 that the intensity of the b branch should also be quite prominent and at about 40 kG would have dominated the a branch in intensity. These serious discrepancies reaffirm that the transitions observed are not transitions between free-carrier states but rather between donor impurity levels.

C. Donor levels (simplified)

We consider the impurity phonon levels

$$E_{\xi_0} = E_{210}, E_{220} ,$$

$$E_{\xi_1} = E_{100}, E_{110}, E_{1\bar{1}0} ,$$

$$E_{\xi_2} = E_{000} .$$

Since the energy difference between (210) and (220) is small throughout the magnetic-field range, we shall consider them together as one level. Similarly the levels (100), (110), and ($1\bar{1}0$) are quite close together, and again we shall consider them degenerate. Hence we have essentially again three levels. Their positions and spectral weight are calculated and presented in Figs. 21 and 22, respectively. To obtain the function $G^{-1}_{\xi_1,q}(E)$ and the spectral weights W_i, we need to calculate the matrix elements of the Fröhlich interaction Hamiltonian between donor impurity variational wave functions (N, M, λ) of the form given in Eq. (1). Explicitly we calculate the quantities

$$|\langle NM\lambda | H_1 | N'M'\lambda'\rangle|^2$$

$$= (\hbar\omega_0)^2 \frac{V}{8\pi^3} \int d^3q \left(\frac{4\pi\alpha}{S}\right) \frac{1}{r_0^2 q^2} |\langle NM\lambda | e^{-i\vec{q}\cdot\vec{r}} | NM\lambda\rangle|^2 . \tag{16}$$

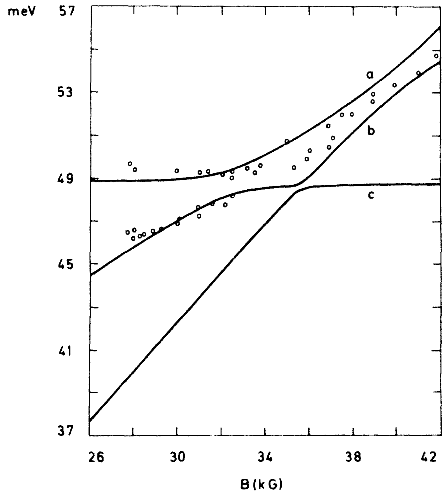

FIG. 21. Interacting levels scheme for bound impurity electrons (simplified).

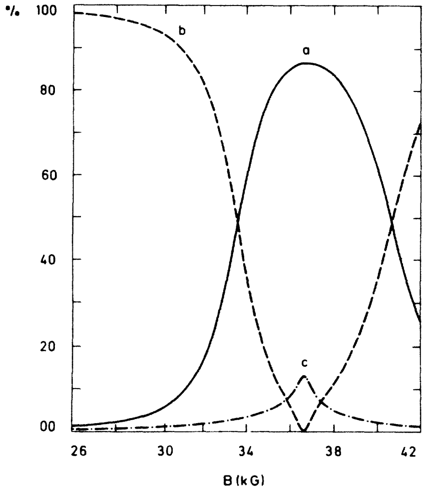

FIG. 22. Absorption intensities of the levels of Fig. 21.

This type of integral can be evaluated by a Bessel function expansion for $\exp(-iq_\perp\rho\cos\phi)$ and utilizing the Laguerre polynomials derivatives. Details together with all the required matrix elements for both Sec. IV C and also Sec. IV D can be found in Appendix B.

Again we have three branches with the polaron-pinning behavior at low fields. Branch c (that corresponds to HCR at low fields) is predicted to have negligible intensity even at 36.5 kG (Fig. 22) in good agreement with experiment. The low-field portion of the b branch fits the data much better than (b) and this improvement is obviously due to the impurity binding energy now included. The gradual transfer of intensity from the a branch to the b branch as B increases beyond 38 kG (Fig. 22) is qualitatively brought out by the switching of the data points from the a branch to the b branch (Fig. 21). It should be emphasized that the transmission dips observed experimentally are quite broad due to lifetime and instrumental broadening. It is difficult to resolve two dips and this hampers detailed comparison between theory and experiment especially on the level positions. We illustrate this point by showing in Figs. 11 and 12 the transmission curves at 39 and 41 kG. At these fields we expect from Fig. 22 two dips of comparable intensities, whereas only one broad dip is observed.

The major discrepancy in this simplified model

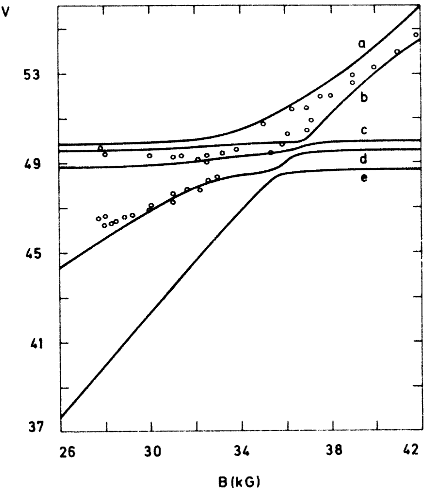

FIG. 23. Detailed interacting levels scheme for bound impurity electrons.

is the lack of correlation between the data points at 35 kG and the *b* branch. We shall see in Sec. IV D that by including the other excited donor levels, this discrepancy can be removed.

D. Donor levels (detailed)

Finally we include the donor excited states $(0\bar{1}0)$, $(0\bar{2}0)$ into the levels already considered in Sec. IV C. These two states together with (000) form three possible states of $|\xi_2;q,q'\rangle$. We compute the magneto-optical spectrum by inserting all the states into Eq. (11) and look for the zeros of $G^{-1}_{\xi,q}(E)$. The results are plotted in Fig. 23 and the spectral weights are shown in Fig. 24. The overall agreement between data and calculated value of positions and intensity variations are improved in this rather complicated scheme. On inspection of the spectral weights in Fig. 24 we can understand that branch *e* is nonobservable; the *d* branch is prominent, less so for both the *a* and *c* branches at low fields; the *a* branch dominates all others at 36.5 kG, and at $B>40$ kG, the *b* branch gains its prominence. All these features are in good agreement with the intensity variations of the observed data. This demonstrates that not only the nonparabolicity but also the detailed donor level schemes play a role in determining the polaron-pinning effects at the two-LO-phonon region.

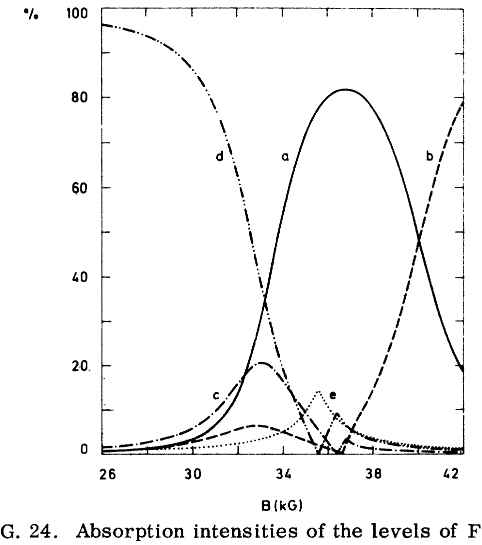

FIG. 24. Absorption intensities of the levels of Fig. 23.

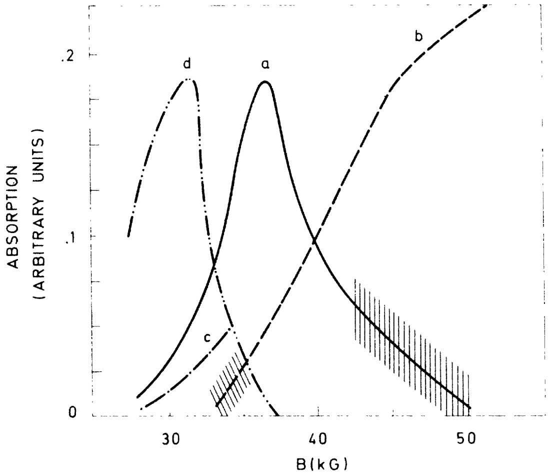

FIG. 25. Experimentally determined absorption intensities of the levels of Fig. 23 sorted out according to procedure described in text. The drop in absorption of branch *d* is possibly due to electron interaction with 2 TO phonons and has not been included in our calculations here.

Guided by the detailed interacting donor levels scheme of Fig. 23, we can assign any data point to the branch that lies closest to it. The measured absorption intensities are determined from the magneto-optical spectrum by integrating the area under the $I(B)/I(0)$ curves. When these experimentally determined absorption intensities sorted out with the help of the levels scheme of Fig. 23 are plotted versus magnetic field, we obtain the results of Fig. 25. We readily see by comparison of Fig. 25 with Fig. 24 that the theoretical and experimental variations of the intensities with field are in remarkably good agreement with each other. This further demonstrates the need to do the detailed interacting donor levels scheme without which the experimental data could never be appreciated as fully as achieved here.

V. SUMMARY AND CONCLUSIONS

In this work we have presented some anomalous and novel features observed in the magneto-optical spectrum of n-InSb in the two-LO-phonon région. These features are far more complicated than the ordinary LO-phonon effects at the one-LO-phonon region. Theoretical analysis is also provided that helps to establish that the electronic levels involved in the transitions observed are donor-impurity states. The transition intensities are attributed to the LO-phonon-assisted cyclotron resonance (LOCR) from the ground state (000) to states like (100) with the emission of one LO phonon. Polaron interaction between electronic states causes complicated modifications of the energy levels including the harmonic cyclotron resonance (HCR) and the ground state plus two LO phonons. Such interactions also induce significant absorption by the harmonic cyclotron resonance which is otherwise too weak to be osberved in the field range of present interest, and by the ground state [or its nearest excited states like (010)] plus two LO phonons, which is otherwise nonabsorptive.

The detailed theoretical analysis demonstrates that the nonparabolicity and the detailed donor levels energy scheme are required to understand the line positions and intensity variations in the magneto-optical spectrum.

Samples of relatively high impurity concentration (1.4×10^{15} cm^{-3}) were used in this work because of the weak absorption intensity of the intraband magneto-absorption relative to the background lattice absorption. In straight cyclotron resonance studies, samples of lower impurity concentration can be used and discrete absorption lines are resolved. In this case, one can sort out free-carrier transitions and satisfy oneself that impurity banding is not excessive.[13] In this work one must conclude that free-carrier transitions are not present, or, if present, they are not resolved. First, the energy positions of the free-carrier transitions were quite precisely established in the earlier work.[13] In the current work, all absorption peaks were observed at higher energies than the free-carrier transitions deduced from the earlier work. The second consideration is that the enormously complicated variations of the data with magnetic field require a theoretical model based upon something more than simple free-carrier transitions. The impurity model fits surprisingly well. Impurity banding effects are probably present and account for the large absorption line widths observed.

It should be pointed out that the experiments reported here were performed a few years ago at M.I.T. Lincoln Laboratory using techniques which can now be improved upon significantly utilizing more recent developments in experimental techniques. Perhaps, since the experimentalist involved in this work has gone on to other things, this paper may inspire others to exploit more modern techniques involving tunable infrared lasers to extend the measurements to samples of lower impurity concentrations. Such advanced experimental work should overcome some of the difficulties with measuring low absorption levels and, with purer samples, may resolve more of the rich structure predicted by the theory.

ACKNOWLEDGMENTS

This work was performed in the framework of the joint project E.S.I.S. (Electronic Structure in Solids) of the University of Antwerpen and the University of Liège. The experimental data reported in this paper was obtained in work performed at MIT Lincoln Laboratory, where the assistance of W. Defeo is gratefully acknowledged. One of the authors (J.T.D.) dedicates this paper to Professor L. P. Bouckaert on the occasion of his seventieth birthday.

APPENDIX A

The perturbed wave function is given by the linear combinations

$$\psi=\sum_{\xi_2}\sum_{\vec{q},\vec{q}'} a(\xi_2;\vec{q},\vec{q}')\,|\xi_2;\vec{q},\vec{q}'\rangle + \sum_{\xi_1}\sum_{\vec{q}} b(\xi_1,\vec{q})\,|\xi_1;\vec{q}\rangle+\sum_{\xi_0} c(\xi_0)\,|\xi_0;0\rangle \qquad \text{(A1)}$$

since

$$H\psi=E\psi\,. \qquad \text{(A2)}$$

Substituting Eq. (A1) into Eq. (A2), multiplying on the left by either $|\xi_0;0\rangle$, or $|\xi_1;\vec{q}\rangle$ or $|\xi_2;\vec{q},\vec{q}'\rangle$ and taking matrix elements, we obtain the set of equations for the coefficients a, b, and c

$$(E-E_{\xi_0})c(\xi_0)=\sum_{\xi_1}\sum_{\vec{q}} b(\xi_1;\vec{q})\langle\xi_0;0|H_1|\xi_1;\vec{q}\rangle \qquad \text{(A3)}$$

$$(E-E_{\xi_1}-\hbar\omega_0)\,b(\xi_1;\vec{q})=\sum_{\xi_0} c(\xi_0)\langle\xi_1;\vec{q}|H_1|\xi_0;0\rangle+\sum_{\xi_2,\vec{q}'} a(\xi_2;\vec{q},\vec{q}')\langle\xi_1;\vec{q}|H_1|\xi_2;\vec{q},\vec{q}'\rangle\,, \qquad \text{(A4)}$$

and

$$(E-E_{\xi_2}-2\hbar\omega_0)\,a(\xi_2;\vec{q},\vec{q}')=\sum_{\xi_1} b(\xi_1;\vec{q})\langle\xi_2;\vec{q},\vec{q}'|H_1|\xi_1;\vec{q}\rangle+\sum_{\xi_1} b(\xi_1;\vec{q}')\langle\xi_2;\vec{q},\vec{q}'|H_1|\xi_1;\vec{q}'\rangle\,. \qquad \text{(A5)}$$

Diagonalizing these matrix equations in the subspace of unperturbed states will determine the perturbed energy E and the coefficients a, b, and c. There will be as many solutions for E as the total number of unperturbed states involved in Fig. 14 for any magnetic-field strength. Neglecting cross terms (which can be interpreted as vertex corrections in the Green's-function language), we get

$$b(\xi_1;\vec{q}) = 2c(\xi_0)\langle \xi_1;\vec{q}\,|H_1|\,\xi_0;0\rangle \Big/ \left(E - E_{\xi_1} - \hbar\omega_0 - \sum_{\xi_2,\vec{q}} \frac{|\langle \xi_2;\vec{q},\vec{q}'\,|H_1|\,\xi_1,q\rangle|}{E - E_{\xi_2} - 2\hbar\omega_0}\right) \tag{A6}$$

and a similar expression for $a(\xi_2;\vec{q},\vec{q}')$ which will not be given here for brevity. In deriving Eq. (A6) we have made the simplifying approximation of lumping both states (210) and (220) for ξ_0 together since they are nearly degenerate and hence summation over ξ_0 is avoided in Eq. (A5). The value of the coefficients, say $b(\xi_i;\vec{q})$ for each branch E_i, can be obtained by substituting E_i for E on the right-hand side of Eq. (A6). The quantities $|b(\xi_i;q)|^2$ will be proportional to the absorption intensity of the ith branch provided that the LOCR dominates the HCR in absorption strength. A procedure such as that described, though it is cumbersome and difficult to attach a physical meaning to the effects of the interaction, will nevertheless yield exactly the same results as the Green's-function approach described in the text.

APPENDIX B

We have to evaluate the electron-phonon matrix element of Eq. (16). Consider first the quantity $\langle NM\lambda|e^{-i\vec{q}\cdot\vec{r}}|N'M'\lambda'\rangle$ that appears in the integral. Let $l \equiv N - \frac{1}{2}(M + |M|)$ the variational wave function of $\langle NM\lambda|$ in Eq. (1) in cylindrical coordinates ρ, φ, and z has the form

$$F(NM\lambda) = \Phi_{lM}(\sigma,\varphi)P_\lambda(z)\exp(-\tfrac{1}{4}\lambda\epsilon^2 z^2) , \tag{B1}$$

where

$$\Phi_{lM}(\sigma,\varphi) = c e^{iM}\sigma^{|M|/2}e^{-\sigma/2}L^{|M|}_{l+|M|}(\sigma) , \tag{B2}$$

where

$\sigma = \frac{1}{2}\gamma\rho^2$, $\gamma = \frac{1}{2}\hbar\omega_c/R^*$ with R^* the effective Rydberg, $L^M_{l+|M|}(\sigma)$ are derivatives associated with the Laguerre polynomials, c is a normalization constant.

$$c^2 = (\lambda/2\pi)l![(l+|M|)!]^3$$

and

$$L^{|M|}_{l+|M|}(\sigma) = (-1)^{|M|}\Gamma(|M|+l+1) \times \sum_{p=0}^{l}(-1)^{l-p}\binom{|M|+l}{p}\sigma^{l-p}/(1-p)! .$$

The matrix element can be written as a product

$$\langle NM\lambda|e^{-i\vec{q}\cdot\vec{r}}|N'L'\lambda'\rangle = \int_{-\infty}^{\infty} dz P_\lambda(z)P_{\lambda'}(z)\exp[-\tfrac{1}{4}(\epsilon^2+\epsilon'^2)z^2 - iq_z z] \times \int_0^\infty\int_0^\pi \rho\,d\rho\,d\varphi\,\Phi_{lM}(\sigma,\varphi)e^{-iq_\perp\rho\cos\varphi}\Phi_{l'M'}(\sigma,\varphi) . \tag{B3}$$

The first integral in Eq. (B3) can be expressed in terms of the integral

$$G(q_z,\alpha) = \int_{-\infty}^{\infty} dz\, e^{-\alpha z^2}e^{-iq_z z} \equiv \frac{\pi}{\alpha}e^{-q_z^2/4\alpha} \tag{B4}$$

and its derivatives

$$\frac{d^n}{dq_z^n}G(q_z,\alpha) .$$

The second integral in Eq. (B3) can be performed by first expanding the factor $\exp(-iq_\perp\rho\cos\varphi)$ in terms of Bessel functions and integrating over φ. Writing out explicitly the derivatives associated with the Laguerre polynomials, the integration over φ is reduced to a sum of integrals of the form

$$K_n(q_\perp) = \int_0^\infty d\rho\,\rho^n e^{-\gamma\rho^2/2}J_{|M-M'|}(q_\perp\rho) . \tag{B5}$$

These integrals have analytical expressions

$$K_n(q_\perp) = [\tfrac{1}{2}|M-M'| + \tfrac{1}{2}(n+1)][q_1/(2\gamma)^{1/2}]^{|M-M'|}/2(\tfrac{1}{2}\gamma)^{1/2(n+1)}\Gamma(|M-M'|+1) \times {}_1F_1[\tfrac{1}{2}|M-M'| - \tfrac{1}{2}n + \tfrac{1}{2};\ |M+M'|+1;\ \tfrac{1}{2}(q_\perp^2/\gamma)] \tag{B6}$$

with

$$ {}_1F_1(\alpha;\beta;z)=\sum_{n=0}^{\infty}\frac{(\alpha)_n}{n!(\beta)_n}\,z^n \tag{B7}$$

$(\alpha)_n$ and $(\beta)_n$ are defined by $(\alpha)_n=\alpha(\alpha+1)\cdots(\alpha+n-1)$; $(\alpha)_0=1$.
Hence the matrix elements $\langle NM\lambda|e^{-i\vec{q}\cdot\vec{r}}|N'M'\lambda'\rangle$ can be obtained analytically.

What remains in the calculation of the right-hand side of Eq. (16) is the integration over $\vec{q}$ which leads to integrals of the form

$$R_n=\int d^3q\,\frac{1}{q^2}\left(\frac{q_\perp^2}{2\gamma}\right)^n e^{-q_\perp^2/\gamma}\,e^{-q_z^2/\gamma\xi^2} \tag{B8}$$

where $\xi^2=\frac{1}{2}(\epsilon^2+\epsilon'^2)$ and n is a positive integer.

By transformation of variables R_n can be reduced to a single integral

$$R_n=\frac{\pi^{3/2}\gamma^{1/2}n!}{2^{n-1}}\int_0^{\infty}dy\,\frac{1}{[y^2+(2/\xi)y+1]^{n+1}} \tag{B9}$$

which can then be obtained by tables of integrals. Our results for the electron-phonon matrix elements as in Eq. (16) are now summarized below:

$$|\langle 100|H_1|000\rangle|^2=\frac{(\hbar\omega_0)^2\alpha}{\pi^2}\left(\frac{r_0}{a_0}\right)\frac{\epsilon_{100}\epsilon_{000}}{\epsilon_{100}^2+\epsilon_{000}^2}\,R_2\ , \tag{B10}$$

$$|\langle 100|H_1|0\bar{1}0\rangle|^2=\tfrac{1}{2}(\hbar\omega_0)^2\,\alpha\left(\frac{r_0}{a_0}\right)\frac{\epsilon_{100}\epsilon_{010}}{\epsilon_{100}^2+\epsilon_{010}^2}\,(R_1-2R_2+R_3)\ , \tag{B11}$$

$$|\langle 100|H_1|0\bar{2}0\rangle|^2=\frac{(\hbar\omega_0)^2}{2\pi^2}\,\alpha\left(\frac{r_0}{a_0}\right)\frac{\epsilon_{100}\epsilon_{020}}{\epsilon_{100}^2+\epsilon_{020}^2}\,(4R_2-4R_3+R_4)\ , \tag{B12}$$

$$|\langle 100|H_1|220\rangle|^2=\frac{(\hbar\omega_0)^2}{2\pi^2}\,\alpha\left(\frac{r_0}{a_0}\right)\frac{\epsilon_{100}\epsilon_{220}}{\epsilon_{100}^2+\epsilon_{220}^2}\,(4R_2-4R_3+R_4)\ , \tag{B13}$$

$$|\langle 100|H_1|210\rangle|^2=\frac{(\hbar\omega_0)^2}{\pi^2}\,\alpha\left(\frac{r_0}{a_0}\right)\frac{\epsilon_{100}\epsilon_{210}}{\epsilon_{100}^2+\epsilon_{210}^2}\,(\tfrac{1}{8}R_1-\tfrac{3}{2}R_2+5R_3-3R_4+\tfrac{1}{2}R_5)\ . \tag{B14}$$

Here

$$r_0=(\hbar/2m^\star\omega_0)^{1/2} \tag{B15}$$

and $m^\star=m_e/68.9$ is the band mass. Taking $\omega_0=24.5$ meV, we obtain $r_0=104$ Å. a_0 is effective Bohr radius and is 600 Å for electrons in InSb.

---

[1] H. Fröhlich, in *Polarons and Excitons*, edited by G. G. Kuper and G. D. Whitfield (Oliver and Boyd, Edinburgh, 1963).

[2] See, for example, articles in *Polarons in Ionic Crystals and Polar Semiconductors*, edited by J. T. Devreese (North-Holland, Amsterdam, 1972).

[3] E. J. Johnson and D. M. Larsen, Phys. Rev. Lett. 16, 655 (1966); D. M. Larsen and E. J. Johnson, J. Phys. Soc. Jpn. Suppl. 21, 433 (1966).

[4] R. Kaplan and R. F. Wallis, Phys. Rev. Lett. 20, 1499 (1968).

[5] C. J. Summers, R. B. Dennis, B. S. Wherrett, P. G. Harper, and S. D. Smith, Phys. Rev. 170, 755 (1968).

[6] D. M. Larsen, *Proceedings of the Tenth International Conference on the Physics of Semiconductors*, edited by S. P. Keller, J. C. Hensel, and F. Stern (U.S. AEC, Washington, D.C., 1970), p. 145.

[7] B. D. McCombe, Proceedings of the Eleventh International Conference on the Physics of Semiconductors, Warsaw, Poland, 1972, p. 321.

[8] D. R. Cohen, D. M. Larsen, and B. Lax, Phys. Rev. B 6, 1367 (1972).

[9] R. Kaplan, K. L. Ngai, and B. W. Henvis, Phys. Rev. Lett. 28, 1044 (1972).

[10] R. Kaplan and K. L. Ngai, Comments Solid State Phys. 5, 157 (1973); 6, 17 (1974).

[11] I. B. Levinson and E. I. Rashba, Sov. Phys. Usp. 16, 892 (1974).

[12] B. D. McCombe and R. Kaplan, Phys. Rev. Lett. 21, 756 (1968).

[13] E. J. Johnson and D. H. Dickey, Phys. Rev. B 1, 2676 (1970).

[14] F. G. Bass and I. B. Levinson, Zh. Eksp. Teor. Fiz. 49, 914 (1965) [Sov. Phys.-JETP 22, 635 (1966)].

[15] A. S. Saleh and H. Y. Fan, Phys. Rev. B 5, 3972 (1972).

[16] J. Van Royen, L. Lemmens, and J. T. Devreese, Solid State Commun. 15, 591 (1974).

[17] R. C. Enck, A. S. Saleh, and H. Y. Fan, Phys. Rev. 182, 790 (1969).

[18] B. D. McCombe, R. J. Wagner, S. Teitler, and J. J. Quinn, Phys. Rev. Lett. 28, 37 (1972).

[19] K. W. Chiu, K. L. Ngai, and J. J. Quinn, Solid State Commun. 10, 1251 (1972).

[20] K. L. Ngai and E. J. Johnson, Phys. Rev. Lett. 29, 1607 (1972).

[21] P. J. Lin-Chung and B. W. Henvis, Phys. Rev. B 12, 630 (1975).

[22] C. R. Pidgeon and S. H. Groves, Phys. Rev. 186, 824 (1969).

[23] R. F. Wallis and H. J. Bowlden, J. Phys. Chem. Solids 7, 78 (1958).